Journal of Environmental Chemical Engineering 9 (2021) 105056

Contents lists available at ScienceDirect

Journal of Environmental Chemical Engineering

journal homepage: www.elsevier.com/locate/jece

Modeling and computational fluid dynamic simulation of acetaminophen adsorption using sugarcane bagasse

Mayra Vera [a], Diego M. Juela [b], Christian Cruzat [a], Eulalia Vanegas [a,*]

[a] Center for Environmental Studies, Department of Applied Chemistry and Production Systems, Faculty of Chemical Sciences, University of Cuenca, Cuenca, Ecuador
[b] Chemical Engineering, Faculty of Chemical Sciences, University of Cuenca, Cuenca, Ecuador

ARTICLE INFO

Editor: V. Victor

Keywords:
Adsorption
Breakthrough curve
Computational fluid dynamic model
Mathematical modeling
Wastewater treatment

ABSTRACT

In this work, the mathematical modeling of acetaminophen (ACT) removal in a fixed-bed adsorption column using sugarcane bagasse (SB) as adsorbent was studied. Experimental data were fitted to six analytical models: Thomas, modified dose-response, Yoon-Nelson, Bohart-Adams, Wang, and Wolborska. Three experimental tests were carried out at 2.5 mL/min of flow rate, 57 mg/L of ACT concentration, and bed heights of 23, 33, and 43 cm. The predicted breakthrough curve by modified dose-response model agreed acceptably ($R^2 > 0.91$) with experimental curves. Besides, a computational fluid dynamic (CFD) model was developed to simulate and analyze the ACT concentration inside of the adsorption column and the wall channeling effect. The simulated breakthrough curve had a good reproducibility with experimental data, the maximum error between experimental and predicted points was 7.03%. In addition, the CFD model shows a high mass transfer zone and a slow adsorption rate in all three tests of ACT adsorption; the mass transfer zone grew as the bed height increased, whereas the wall channeling effects disappeared with increasing bed height. Also, the diffusion resistances and axial dispersion phenomenon were relevant. The results of this research work demonstrate the usefulness of computational fluid dynamics analysis to understand better the adsorption process.

1. Introduction

Currently, the study of emerging pollutants is among the priority research lines of the main agencies dedicated to the protection of public health and the environment, such as the World Health Organization (WHO), the Agency for the Protection of Environment (EPA), and the European Commission [1,2].

The appearance of emerging pollutants and the variation in concentrations has its origin in the so-called water cycle. In concordance to this cycle, the main way of entry of pollutants into the aquatic environment is wastewater, which includes that of urban, industrial, agricultural, or livestock origin [3,4]. The prevalence of one or other depends largely on the type of contamination in question, as well as on the level of purification or natural attenuation that they experience. Somewhere in this cycle, in which different environmental compartments and human activities converge, is where the alteration of water quality occurs [5–7].

Pharmaceuticals are among the emerging pollutants that have increased rapidly in recent decades, providing better quality health for humans and animals. After use, large quantities of pharmaceutical products are discharged into bodies of water and are therefore detected in wastewater, increasing microbial resistance and bioaccumulation [8–11].

Conventional wastewater treatments are ineffective in removing and/or degrading most of the emerging contaminants. Particularly, acetaminophen (ACT), is one of the most used pharmaceutical products by the population, it has been found in surface and underground water bodies: 186.5 μg/L in hospital wastewater, 15.7 μg/L in surface water of rivers, and 417.5 μg/L in effluents from drug production plants [12–14]. In Scotland, ACT was found at the inlet and outlet of a wastewater treatment plant at a concentration of 492–6924 ng/L, and 11.733 ng/L, respectively. This indicates that although ACT presents a high percentage of removal, it is not completely eliminated with conventional treatment. In the United States, it was detected in 24% of 139 analyzed effluents[15–17].

In recent years, the use of both oxidation and membrane filtration processes has been studied. Also, cheaper technologies such as subsurface flow wetlands and biosorption have been extensively studied [18]. The use of biosorption for the removal of pharmaceutical compounds present in wastewaters is of special interest due to the abundant types of

* Correspondence to: University of Cuenca, Av. 12 de Abril, 010203 Cuenca, Ecuador.
E-mail address: eulalia.vanegas@ucuenca.edu.ec (E. Vanegas).

https://doi.org/10.1016/j.jece.2021.105056
Received 28 September 2020; Received in revised form 3 January 2021; Accepted 7 January 2021
Available online 12 January 2021

biomass y and high removal percentages. Currently, a large number of low-cost biomaterials are being studied and have the potential to be used as biosorbents, among which we can mention: vegetal remains, algae, fungi, arthropod shells, bacteria, etc., which are found in great abundance and are easily transformable to biosorbent agents [19–21].

Most of the studies on biosorption that appear in literature have been carried out in discontinuous systems, although from a practical point of view, biosorption processes on a large scale are carried out in a continuous way, generally in fixed-bed columns. To design effective packed bed units with solid adsorbent, mathematical models that can successfully simulate experimentally obtained breakthrough curves are required. These models must predict the dynamics of the adsorption or ion exchange process to facilitate the development of novel applications, such as the design of columns packed with biosorbent material to remove pharmaceutical residues from industrial wastewater [22–28].

Several fixed-bed adsorption models with explicit equations have been widely used to describe the behavior of the breakthrough curve, including the Bohart–Adams, Thomas, Yoon–Nelson, Clark, Wolborska, and Modified dose-response models. These simplified models are primarily established according to the description of mass transfer within adsorption systems and they can describe the experimental data satisfactorily for most practical design purposes.

Computational modeling has become an essential part of science and engineering. In recent years software capable of simulating many of the physical and chemical processes that take place in laboratories, pilot plants, and industrial processes have been developed. The use of COMSOL Multiphysics allows profitable savings in operational processes and predicts the behavior of the breakthrough curve by considering the main phenomena in a fixed-bed column [29–32].

The main objective of this work was to evaluate the technical viability of using sugarcane bagasse as an adsorbent in the removal of ACT; the modeling of the breakthrough curve by applying different mathematical models and simulation with a computational fluid dynamic model solved with COMSOL Multiphysics were also studied.

2. Materials and methods

2.1. Materials

Acetaminophen (ACT), ($C_8H_9NO_2$), with a molecular weight of 151.17 g/mol, logarithmic of the dissociation constant (pK_a) 9.5 and 5.7, octanol-water partition coefficient (log Kow) equal to 0.89 was supplied by Sigma Aldrich. All ACT solutions were prepared with distilled water at an initial concentration of 57 mg/L, and with 1% of methanol (Sigma Aldrich, HPLC grade). The pH of the ACT solutions was adjusted to 6 with HCl supplied by Merck in a 0.1 N solution. All chemical reagents used in this study were of analytical grade.

Sugarcane bagasse (SB) was acquired at Yunguilla mills, Cuenca, Azuay, Ecuador. The SB was chosen in good conditions of conservation and the bark was separated from the pulp. The pulp was washed several times with drinking water to remove all kinds of impurities, then it was dried in the open air to decrease the amount of moisture, and then the drying was completed in the oven at 60 °C for 8 h. Finally, it was crushed with a manual mill and sieved through a N° 20 sieves, from which particles with a diameter of 0.59 mm were obtained.

2.2. Adsorption experiments

The experimental adsorption test was performed using a glass burette with an inner diameter of 1.5 cm and a height of 50 cm. The column was packed with SB until reaching a bed height of 23, 33, and 43 cm. The solution was pumped at a flow rate of 2.5 mL/min controlled by a peristaltic pump. All the samples concentration was measured using a UV-Vis spectrophotometer. The breakthrough time and the saturation time were established when the effluent ACT concentration reaches 5% and 80% of the inlet concentration, respectively.

2.3. Fixed-bed adsorption modeling

As one of the most prevalent techniques for separation and purification, fixed-bed adsorption has been widely applied for its high efficiency and easy operation. Given the fact that the experimental determination of adsorption performance under various conditions is often costly and time-consuming, the development of mathematical models is necessary to predict fixed-bed adsorption.

The performance of a fixed-bed column can be predicted through a mathematical modeling approach of breakthrough curves. Among the most used mathematical models to describe the dynamic behavior of pollutant removal in a fixed-bed column are the Bohart-Adams, Thomas, Yoon-Nelson, Wang, Wolborska, and modified dose-response models. These models were applied to the experimental data obtained for the biosorption of ACT with SB.

2.3.1. Thomas model

The Thomas model is frequently applied to estimate the adsorptive capacity of an adsorbent and predict breakthrough curves. It assumes the second-order reversible reaction kinetics and the Langmuir isotherm. Theoretically, it is suitable to estimate the adsorption process where external and internal diffusion resistances are extremely small [33,34]. The Thomas model is given by Eq. (1).

$$\ln\left(\frac{C_i}{C}-1\right)=\frac{k_{Th}q_F m}{Q}-k_{Th}C_i t \tag{1}$$

Where, C is the ACT concentration at the outlet of the column (mg/L), C_i is the initial concentration of ACT (mg/L), t is the sampling time (min), k_{Th} is the Thomas rate constant, m is the adsorbent mass packed into the column, and q_F is the adsorption capacity (mg/g) The parameters k_{Th} and q_F were obtained from the slope and the intercept of the plot $ln\ [(C_i/C) - 1]$ versus t.

2.3.2. Modified dose-response model

This model has been commonly used in pharmacology to describe different types of processes. It is currently being used to describe the column biosorption processes, and its importance lies in describing the complete breakthrough curve with great accuracy, as well as minimizing the errors that result from using the Thomas model, especially at low or high times of removal [35,36]. This model is expressed by Eq. (2).

$$\frac{C}{C_i}=1-\frac{1}{1+\left(\frac{C_i Q t}{q_F m}\right)^{a'}} \tag{2}$$

Representing $\ln(C/C_i - C)$ versus t, we can obtain the values of the parameters of the model, a' and q_F, from the slope and the ordinate to the origin. Where a is the model constant and q_F is the maximum concentration of solute in the solid phase (mg/g).

2.3.3. Yoon-Nelson model

The Yoon-Nelson model is extremely concise in form, supposing that the decrease in the probability of each adsorbate to be adsorbed is proportional to the probability of its adsorption and breakthrough on the adsorbent [37,38]. It can be represented by Eq. (3).

$$In\left(\frac{C_i}{C}-1\right)=K_{YN}\tau-K_{YN}t \tag{3}$$

Where K_{YN} is the proportionality constant of Yoon-Nelson (min^{-1}) and τ is the time when $C/C_i = 0.5$ (min).

2.3.4. Bohart-Adams model

The Bohart-Adams model [39] was developed based on the assumption that the adsorption rate is proportional to the adsorbent's residual capacity and the adsorbate's concentration [40]. This model

has been extensively applied in other various systems [41,42]. The expression is given as follows in Eq. (4).

$$\ln\left(\frac{C_i}{C}-1\right)=\frac{k_B q_m H}{u}-k_B C_i t \tag{4}$$

Where, k_B is the kinetic constant of the Bohart-Adams model (L/mg min), H is the bed height (cm), q_m is the adsorption capacity by per bed volume (mg/L), and u is the superficial velocity of ACT solution within the packed bed column (cm/min). The parameters k_B and q_m were determined from the intercept and slope of the linear plot of $ln\left(\frac{C_i}{C}-1\right)$ against time (t), respectively.

2.3.5. Wang model

This model is relatively new, it was proposed by Wang et al. [43]. This model assumes an isothermal adsorption process, negligible axial dispersion, and that the breakthrough curve is symmetric. It can be expressed by Eq. (5).

$$t=\tau+\frac{1}{k_w}ln\left(\frac{X}{1-X}\right) \tag{5}$$

Where X is C/C_i ratio, k_w is the kinetic constant (min^{-1}), and τ is the time in which the adsorbate concentration at the outlet of the column reaches half the feed concentration (min). The parameters k_w and τ can be found with the slope and intercept of the graph t versus $ln\ [X/(1-X)]$, respectively. The disadvantage of this model is that, like the Yoon-Nelson model, it does not provide complete information on the adsorption process.

2.3.6. Wolborska model

Wolborska [44], and Pustelnik [46] analyzed the adsorption of *p*-nitrophenol on activated carbon. They found that the initial segment of the breakthrough curve is controlled by film diffusion with a constant kinetic coefficient, and the concentration profile of the initial stage moves axially in the column at a constant velocity. Moreover, the width of the concentration profile in the column and the final breakthrough curve was nearly constant. Based on the above observations, they developed a model to describe the breakthrough at the low concentration region, which was written as shown in Eq. (6) [44–46].

$$\ln\left(\frac{C}{C_i}\right)=\frac{\beta_L C_i \varepsilon}{\rho q_F}t-\frac{\beta_L H}{u} \tag{6}$$

Where, β_L is the film diffusivity (min^{-1}), q_F is the adsorption capacity provide by the Wolborska model (mg/g), and ε is the bed void fraction. The parameters q_F and β_L were estimated through the slope and intercept of the plot $ln\ (C/C_i)$ vs. t with experimental data.

2.4. Computational fluid dynamic (CFD) model

The dynamic behavior of ACT molecule into the fixed-bed column of SB was studied using an integrated CFD model. The following assumptions were considered to formulate the ACT-SB adsorption mechanism.

1) The CFD model includes expressions for fluid dynamics and ACT mass transfer.
2) The adsorption system operates under isothermal conditions.
3) Plug flow with axial dispersion was considered in the behavior of the fluid.
4) There is a concentration gradient of ACT only in the longitudinal direction of the bed, and it is neglected in the radial direction.
5) The rate of adsorption of ACT is described by the linear driving force model (LDF).
6) The adsorption equilibrium is described by the Langmuir nonlinear isotherm.
7) The global mass transfer coefficient includes external fluid film resistance and macropore diffusion.
8) The SB pore diameter is considered to be slightly larger than the ACT molecule (5.48 > 0.46 nm), therefore Knudsen diffusion was taken into account [64].
9) The particle bed has a constant cross-section throughout the bed.
10) The SB particles are considered spherical, and homogeneous in size and density.

2.4.1. Fluid dynamics

The Brinkman-Forchheimer model was used to simulate the flow of the ACT solution in the SB porous medium. This model includes continuity and Navier-Stokes equations, and these are described as shown in Eqs. (7) and (8), respectively.

$$\frac{\partial(\varepsilon_b \rho)}{\partial t}+\nabla(\rho u)=0 \tag{7}$$

$$\frac{\rho}{\varepsilon_b}\left(\frac{\partial u}{\partial t}+(u.\nabla)\frac{u}{\varepsilon_b}\right)=$$

$$-\nabla P+\nabla\left[\frac{1}{\varepsilon_b}\left\{\mu\left(\nabla \mathrm{u}+(\nabla \mathrm{u})^T\right)-\frac{2}{3}\mu(\nabla.\mathrm{u})\right\}\right]-\left(\kappa^{-1}\mu\right)u+F \tag{8}$$

In these equations, μ is the dynamic viscosity of the ACT solution (kg/m.s), u is the velocity vector (m/s), ρ is the density of the ACT solution (kg/m^3), P is the pressure (Pa), ε_b is the bed void fraction, κ is the permeability tensor of the SB porous medium (m^2), and F stands for the volume force of the regions ($kg/m^2.s^2$). Permeability was obtained from Ergun's equation [47,48].

2.4.2. ACT transport and adsorption

The general mass balance equation for the transport and adsorption of diluted species in porous media when the pore space is primarily filled with liquid but also contains pockets or immobile gas is described as shown in Eq. (9).

$$\frac{\partial(\varepsilon_b C)}{\partial t}+\frac{\partial(\rho_b q)}{\partial t}-\nabla(D_z-D_e)\nabla C+\quad v_i\nabla C=R \tag{9}$$

On the left side, the first two terms correspond to the ACT concentration within the liquid and solid phase, the following term introduces the dispersion (D_z), and volatilization (D_e) phenomenon in the x, y, and z directions. While the last term describes convection. On the right-hand side, R describes the rate of the adsorption reaction. The volatilization and reaction adsorption were neglected ($D_e = 0$, $R = 0$) for being a little influential in aqueous phase adsorption. Also, in Eq. (9), C is ACT concentration in the liquid phase (mol/m^3), ρ_b is the bulk density (kg/m^3), and D_z is the axial dispersion coefficient (m^2/s).

The mass transfer rate was described using the linear driving force (LDF) model:

$$\frac{\partial q}{\partial t}=K_i\left(q_e-q\right) \tag{10}$$

Where K_i is the global mass transfer coefficient (s^{-1}), q_e is the ACT concentration in the solid phase at equilibrium (mol/kg). The parameter q_e was calculated from the Langmuir nonlinear isotherm, Eq. (11).

$$q_e=\frac{q_{max}k_L C_e}{1+k_L C_e} \tag{11}$$

Where, k_L and q_{max} are the Langmuir constant (m^3/mol) and the maximum adsorption of the solid phase in monolayer (mol/kg), respectively. These parameters were obtained by previous batch studies.

The missing parameters: K_i,Dz, Knudsen diffusion coefficient (D_k), and ACT molecular diffusion coefficient (D_m), were estimated by empirical correlations drawn from different studies [32,49–51], and are

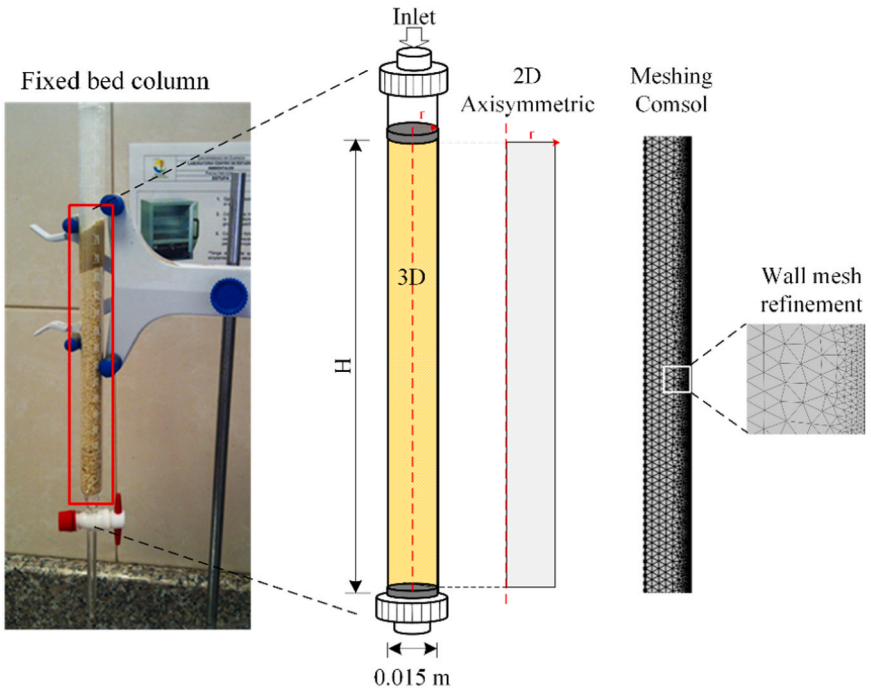

Fig. 1. Reduction of 3D to 2D geometry of the adsorption column.

shown in Eqs. (12)–(15), respectively.

$$\frac{1}{K_i} = \frac{R_P}{3k_{fi}} + \frac{R_p^2}{15\varepsilon_p D_p} \tag{12}$$

$$\frac{v_i d_p}{D_z} = 0.2 + 0.011\left(\frac{Re}{\varepsilon_b}\right)^{0.48} \tag{13}$$

$$D_k = 97 r_p \left(\frac{T}{M_s}\right)^{0.5} \tag{14}$$

$$D_m = 7.4{*}10^{-8}\frac{(\alpha_A M_s)^{0.5} T}{\eta_s V_m^{0.6}} \tag{15}$$

Where, k_{fi} is the external film mass transfer coefficient (m/s), D_p is the effective pore diffusivity coefficient (m^2/s), ε_p is the particle porosity, d_p is the adsorbent particle diameter (m), M_s (g/mol), η_s (kg/m.s) and α_A are the molecular weight, the dynamic viscosity, and the solvent association factor, respectively; V_m is the solute molar volume at its normal boiling point (cm^3/mol), T is the solution temperature (K), R_p is the radius of the adsorbent particle (m), and r_p is the pore radius (m).

Additionally, the CFD model analyzed the wall channeling effect. A space-depended function was used to describe the bed porosity distribution, namely, the bed porosity varies with radial distance from the column according to Eq. (16) [52].

$$\varepsilon_b(r) = \left[1 + \frac{1-\varepsilon_b}{\varepsilon_b}\left(1 - e^{-2(R-r)}\right)^{1/2}\right]^{-1} \tag{16}$$

Where, R is the radius of the fixed-bed column (m), and r is the radial distance from the center of the bed (m).

2.4.3. Numerical solution

The CFD model was implemented and solved numerically in COMSOL Multiphysics V5.4. The column geometry was reduced from 3D to 2D axisymmetric model, as can be seen in Fig. 1. The transport of diluted species in porous media module was used to represent the ACT transport equation, and the PDE module was used to describe the LDF model. Additionally, the Brinkman equations module was used to describe the flow of the ACT solution in the SB. Finally, the 2D axisymmetric model was meshed by free triangular mesh [53–55]. Additionally, to analyze the wall channeling effect, the mesh was refined manually at the wall, as can be seen in Fig. 1. A mesh-size independence study was carried out using a systematic mesh refinement and analyzing ACT concentration difference (%). A grid-independent solution was obtained with a total mesh of 9 483 elements, 0.031% of concentration difference, and a computational time of 4.52 min, which was eventually used in the CFD simulations.

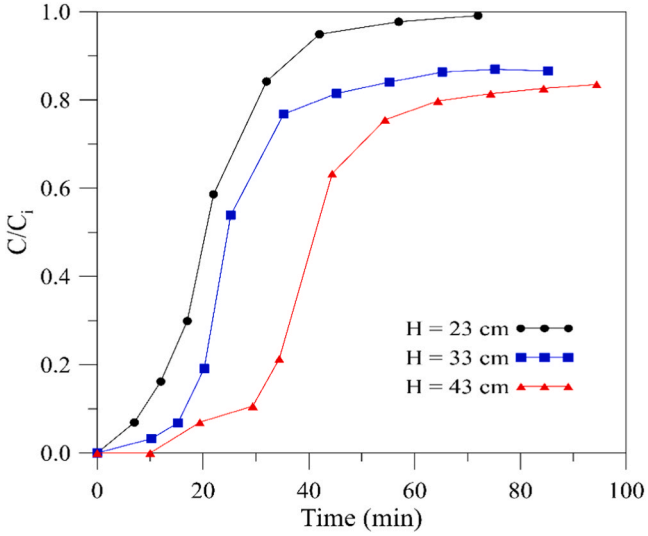

Fig. 2. ACT breakthrough curve with sugarcane bagasse.

3. Results and discussion

3.1. Biosorption tests in columns: Analysis of the breakthrough curve

To analyze the removal of ACT in a fixed-bed column, the final and

Table 1
Parameters of Analytical models.

Model	Parameter	H = 23 cm	H = 33 cm	H = 43 cm
Experimental	q_F (mg/g)	0.447	0.553	0.647
	τ (min)	20.59	24.67	41.24
Yoon Nelson	k_{YN} (min^{-1})	0.095	0.066	0.059
	τ (min)	23.25	39.23	52.41
Thomas	k_{Th} (mL/mg min)	1.668	1.150	1.040
	q_F (mg/g)	0.549	0.663	0.680
Modified dose-response	a	3.243	2.684	3.082
	q_F (mg/g)	0.439	0.539	0.606
Bohart-Adams	k_B (mL/mg min)	1.668	1.150	1.040
	q_m (mg/L)	81.11	96.22	98.66
Wolborska	β_L (min^{-1})	0.108	0.107	0.089
	q_F (mg/g)	1.359	1.011	0.923
Wang	k_w (min^{-1})	0.104	0.089	0.073
	τ (min)	24.65	40.29	53.00

initial concentration ratio (C/C_i) was plotted versus time (min), with an initial concentration of 57 mg/L, flow through the column of 2.5 mL/min, pH of 6, and bed heights of 23, 33 and 43 cm. The results are illustrated in Fig. 2.

The breakthrough curve obtained for ACT is similar to the breakthrough curve reported in Lorphensri [56]. From the breakthrough curve, several data that are necessary for mathematical modeling are obtained. An increase in bed height significantly prolongs the breakthrough and saturation time of the column. For instance, saturation and breakthrough times at 23 cm were around 6 and 42 min, respectively, whereas at 43 cm these were 17 and 66 min, respectively. This is because at 43 cm there is more SB, and hence more active sites available to remove ACT [56]. As a consequence, the adsorption capacity increased with bed height (Table 1). The experimental breakthrough curves obtained have a sigmoidal shape, which indicates that the ACT adsorption into SB is an ideal system. Furthermore, the three breakthrough curves have a low slope and are similar to each other, which indicates that the mass transfer mechanism is controlled by diffusion, as proposed in the CFD model.

The removal of ACT has been studied by using coconut mesocarp in a batch process, obtaining satisfactory results [57]. In the study carried out by Flores [58], the ACT removal efficiency in a fixed-bed column was evaluated, using SB and vegetal sponge against activated carbon. The results showed that SB is more convenient than activated carbon in terms of price and efficiency, with 60% adsorption against 45% adsorption of activated carbon, while the sponge was responsible for eliminating 40% of the ACT dissolved in enriched water samples [58].

3.2. Adjustment of experimental data to the mathematical models

In this work, six analytical models have been applied to reproduce the experimental breakthrough curve, Thomas, Bohart-Adams, modified dose-response, Yoon-Nelson, Wolborska, and Wang models. The corresponding linear plot and breakthrough curves are shown in Figs. 3–5.

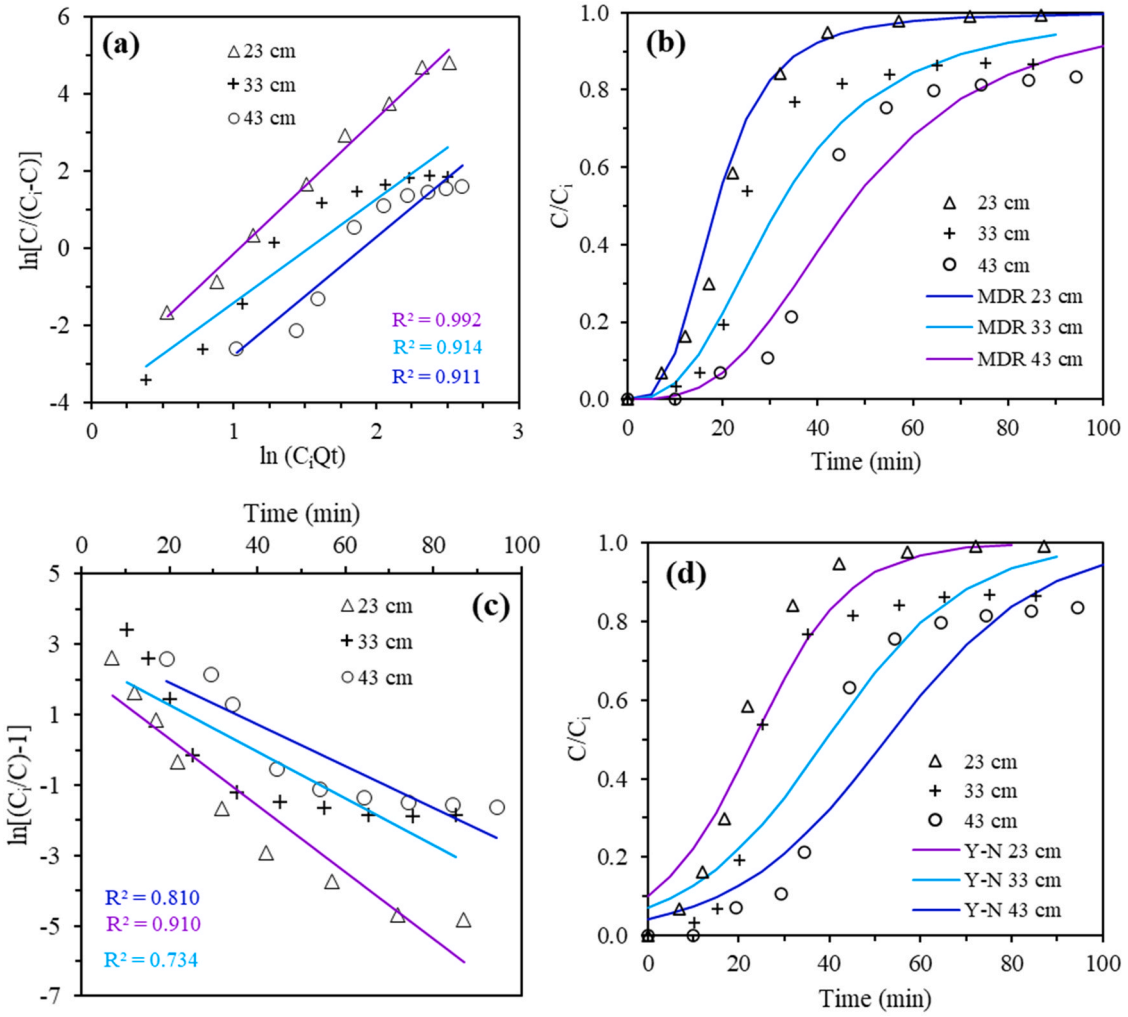

Fig. 3. Linear plot and breakthrough curves for modified dose-response (a and b) and Yoon Nelson models (c and d).

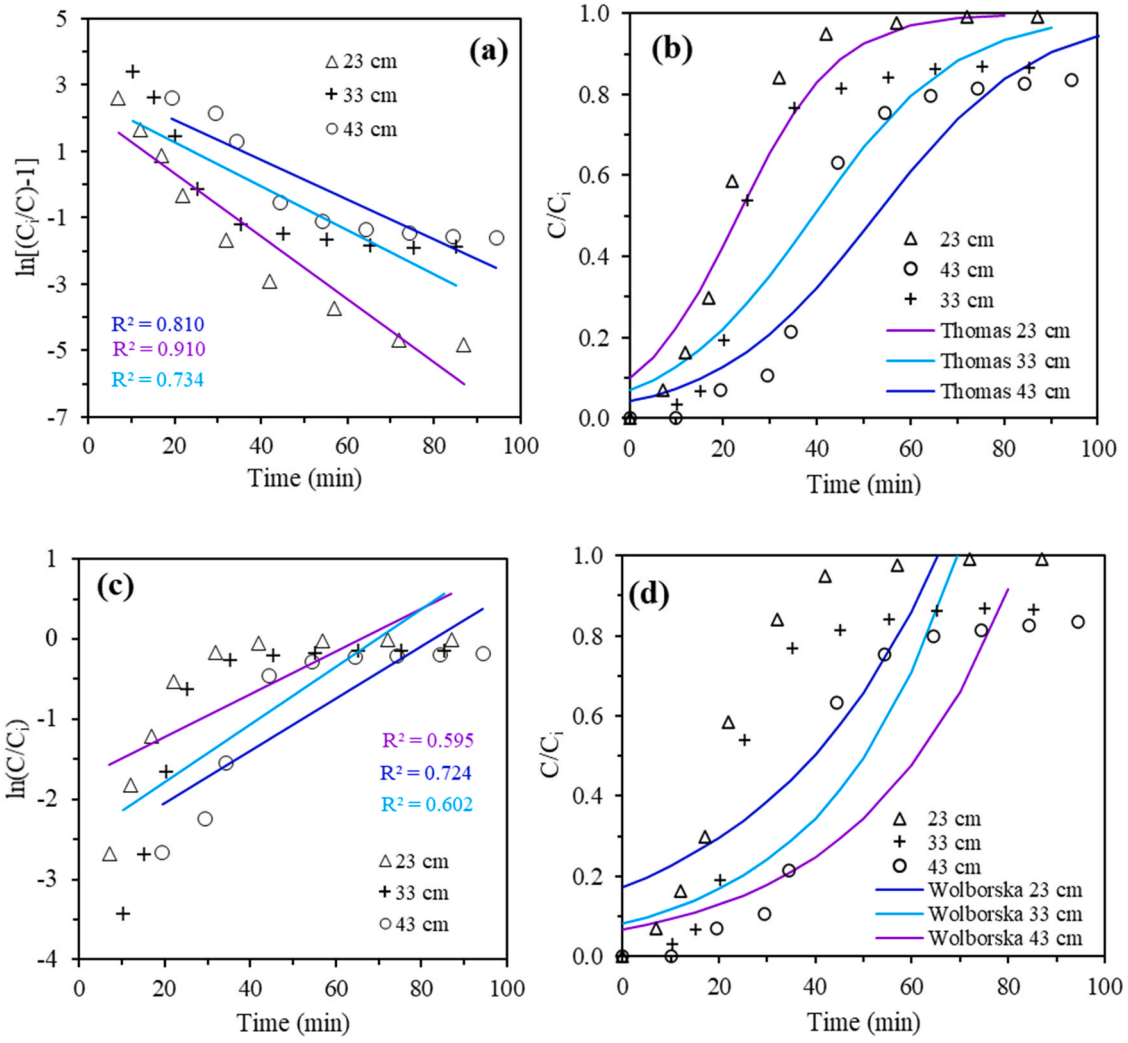

Fig. 4. Linear plot and breakthrough curves for Thomas (a and b) and Wolborska models (c and d).

As can be seen, the modified dose-response (MDR) model was the best that reproduced the experimental data. The correlation coefficient (R^2) for this model was greater than 0.9 in all three studies. For the Thomas, Yoon-Nelson (Y-N), Bohart-Adams (B-A), and Wang models, R^2 values were similar in each test, and are in the range of 0.72–0.91. The fact that the values of R^2 were similar is due to the fact that the equations of these four models are mathematically equivalent [59]. The worst adjustments with the experimental data were obtained with the Wolborska model with $R^2 < 0.72$.

Fig. 3a and b show the linear plots and breakthrough curves obtained with the modified dose-response model. This model was the one that best described the experimental data suggesting its suitability to be used for the design and scaleup purpose. Its importance is that it describes the complete breakthrough curve with great accuracy, and can also minimize the errors that result from using the Thomas model, especially at low or high removal times. Table 1 shows the parameters of the modified dose-response model. The maximum concentration of solute in the solid phase q_F (mg/g) increased as the bed height increased, which was very similar to experimental behavior. Through the parameters found with this model, it is possible to obtain an expression that reproduces the behavior of the columns in other experimental conditions, without the need to carry out other experiments.

As for the rest of the models, their low fit can be mainly due to two reasons: First, the assumptions of the models do not agree with the actual adsorption mechanisms of ACT and therefore these fail in predict the breakthrough curve. This may be the case of the Wolborska, Bohart-Adams, and Thomas models. Second, the model does not take into account information on the adsorbate and adsorbent properties, and therefore it is less accurate in predicting the breakthrough curve under a variety of conditions [23]. This may be the case with the Yoon Nelson and Wang models.

The breakthrough curve obtained with the Wolborska model had a low fit to the experimental curve. Although this model was initially proposed to describe the initial part of the breakthrough curve, its fit is not good even in this section for the present study as can be seen in Fig. 4d. This model assumes that the adsorption is controlled by film diffusion with a constant kinetic coefficient. As will be discussed later, the CFD simulation shows that film diffusion is irrelevant, whereas the external and internal diffusion resistances are predominant. The parameters, β_L and q_F of the Wolborska model are shown in Table 1. Due to the low fit, the adsorption capacity predicted by this model has an opposite effect to that observed in experimentation, since q_F decreases with increasing bed height.

On the other hand, the Bohart-Adams model assumes negligible axial dispersion and mass transfer; therefore, similar assumptions are considered in the Thomas model. Basically, it assumes pseudo-second-order kinetics, insignificant axial dispersion, and a Langmuir isotherm. Also, this model considers extremely small external and internal diffusion resistances. Their low R^2 values again indicate that the assumptions of these models do not fully agree with the actual adsorption process of

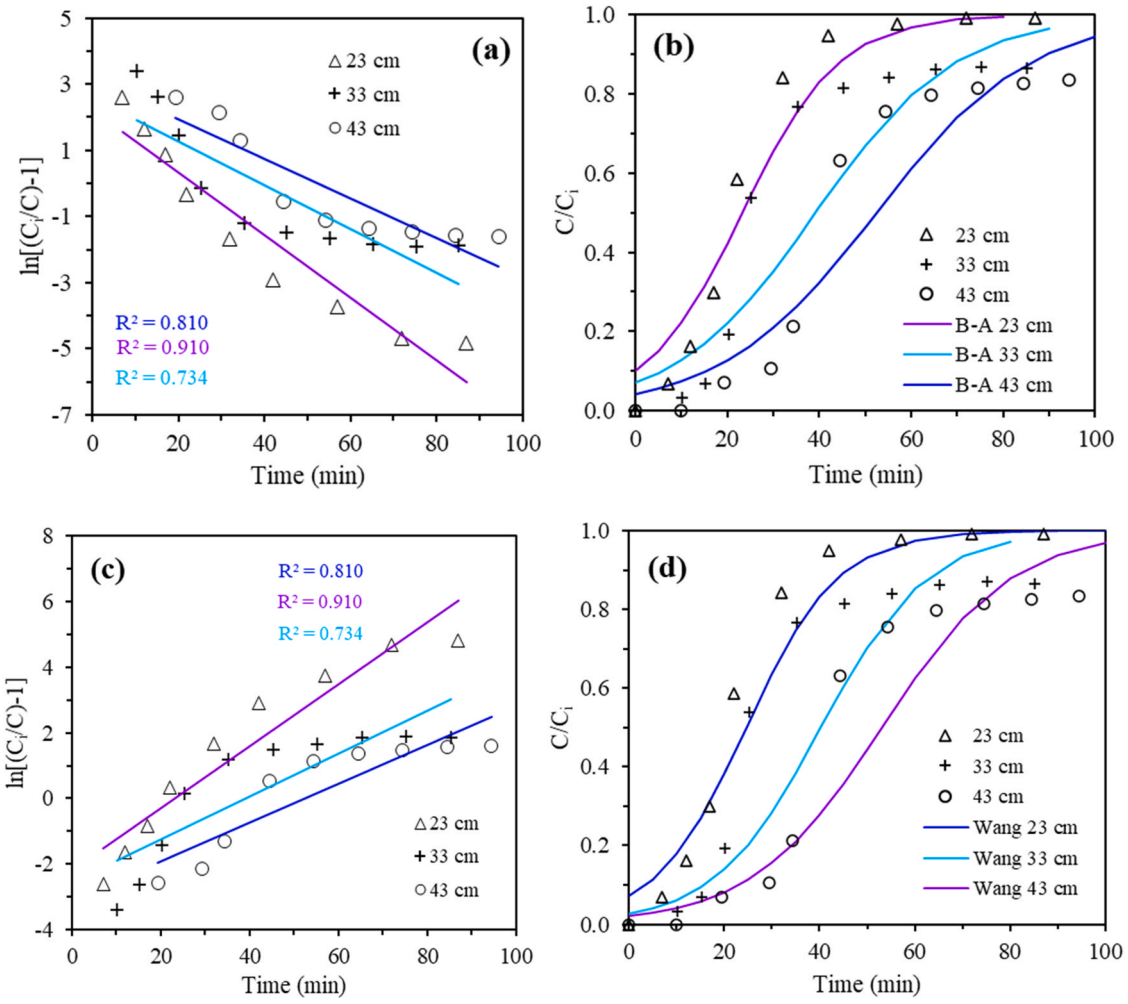

Fig. 5. Linear plot and breakthrough curves for Bohart-Adams (a and b) and Wang models (c and d).

ACT in SB. The diffusion resistance and axial dispersion phenomenon are very relevant in the ACT adsorption into SB, as will be seen later. The parameters of these models are shown in Table 1; it was observed that the kinetic constant of both models (k_{Th} and k_B) was similar in all three studies, and it decreased with increasing bed height, which means that the speed with which ACT passes from the liquid to the solid phase decreases when there is a greater amount of SB [56,57].

Regarding the Yoon-Nelson and Wang models, these models are similar in their form with similar parameters. Although equal values of R^2 were obtained in both models, the values of τ and the rate constant (k_{Th} and k_w) were different (Table 1). The time required for 50% ACT adsorption with the Yoon Nelson model was very close to the experimental value, and it was lower than that obtained by the Wang model in all three tests. Similarly, the kinetic constant of the Wang model was higher than the Yoon-Nelson model, and its effect with bed height is similar to that of the Bohart-Adams and Thomas models. Finally, the predicted breakthrough curves of the Wang model were slightly different from those of the Yoon-Nelson, Bohart-Adams, and Thomas models although equal values of R^2 were obtained.

3.3. CFD simulation

The breakthrough curves predicted by the CFD model were compared with experimental data obtained at a flow rate of 2.5 mL/min, ACT initial concentration of 57 mg/L, bed heights of 23, 33, and 43 cm, as shown in Fig. 6.

Based on the results, the predicted data demonstrated a good agreement with experimental data. The simulated and experimental breakthrough curves converge in almost the entire trajectory with slight variations in the final region, especially at 33 and 43 cm of bed height, hence the saturation time varies significantly from the experimental value. On average, the error between the experimental and predicted points was 1.5% for 23 cm, 7.03% for 33 cm, and 5.98% for 43 cm. For the predicted breakthrough curves at 33 and 43 cm, the error was higher than 5%, which means that the model does not accurately correlate with breakthrough data, especially in the final region. This deviation could be due to two possible reasons. The main justification is due to the fact that at these bed heights, the experimental breakthrough curves show asymmetric tail behavior (i.e., a slow approach of C/C_i toward unity). However, the presented CFD model does not take into account any consideration for this phenomenon; so, for further refinement of the model, the factors responsible for the tailing behavior should be considered [60]. Similar behavior was found in a mechanistic model for the copper adsorption [61]. The second reason with less likely could be the axial dispersion; at these bed heights, this effect could be not significant, so the assumptions of the model fail at these conditions [62]. Despite the deviations, the CFD model, the assumptions, and the correlations used are quite consistent in the initial and transition region of the curves, which could be useful when in practice the adsorbent bed is replaced before a breakthrough of more than 50%. The axial dispersion coefficient and the global mass transfer coefficient estimated by empirical correlations, and were 0.0291 s^{-1}, and 3.68×10^{-7} m^2/s, respectively. Also, the Knudsen diffusion coefficient had a significant value compared to pore diffusion ($1.07 \times 10^{-6} > 4.95 \times 10^{-10}$ m^2/s).

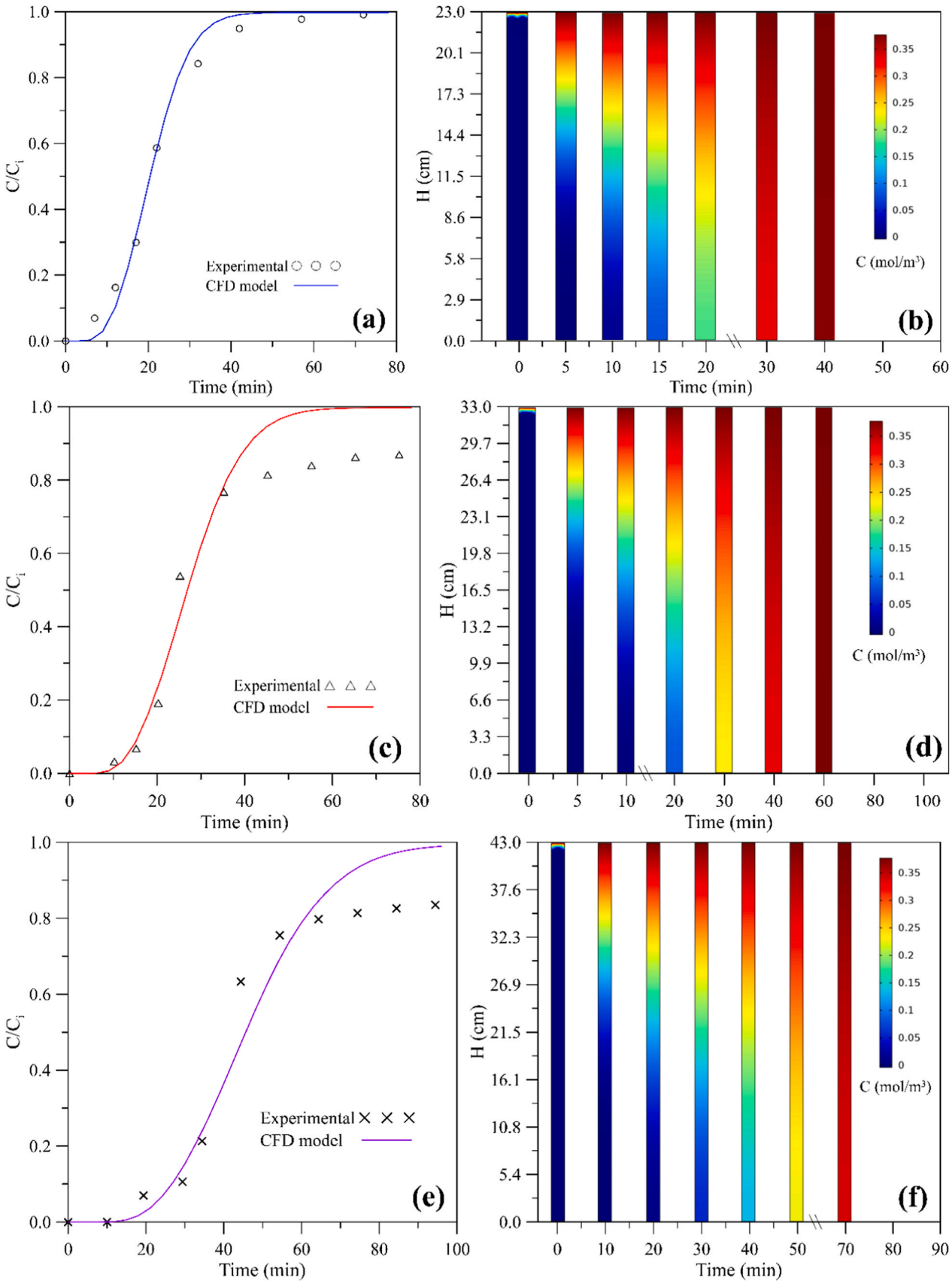

Fig. 6. Simulated and experimental breakthrough curves for ACT adsorption at a bed height of 23 cm (a and b), 33 cm (c and d), and 43 cm (e and f).

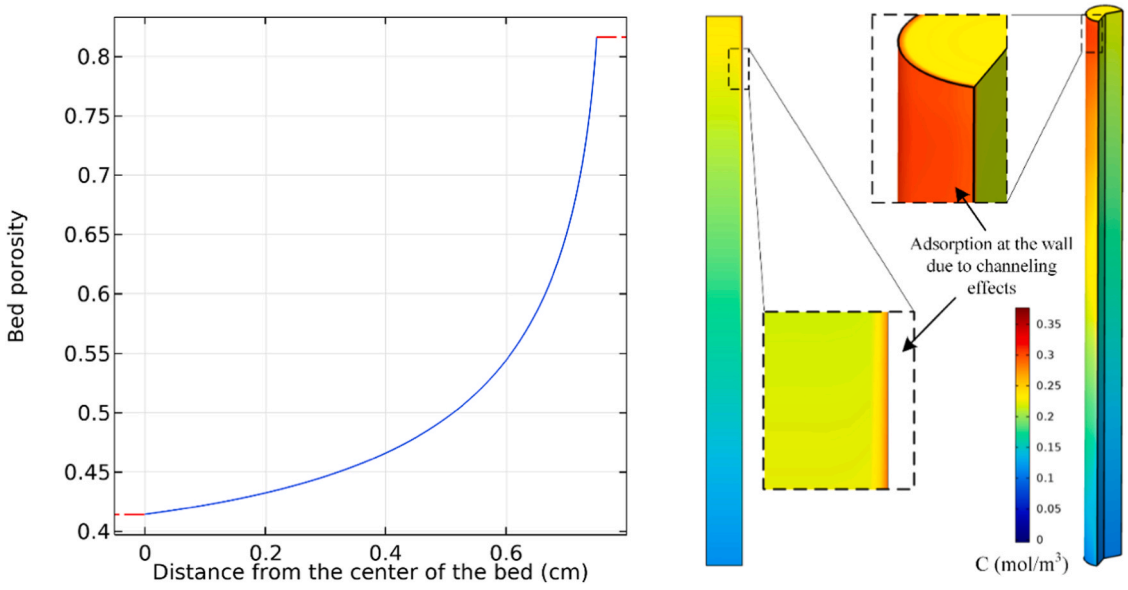

Fig. 7. The porosity distribution (left), and wall channeling effect in the fixed-bed column (right).

This is because the pore size of SB is only slightly greater than the diameter of the ACT molecule, which implies that Knudsen diffusion plays a more significant role in ACT adsorption with SB [66].

The variation of ACT concentration in the longitudinal and radial direction inside of the fixed-bed column was studied with the CFD model, and it is shown in Fig. 6b, d, and f, for 23, 33, and 43 cm of bed height, respectively. For a bed height of 23 cm, the ACT concentration profile was studied at 0, 5, 10, 15, 20, 30, and 40 min. A color scale is shown to indicate the ACT concentration value through the SB fixed-bed, where 0.377 mol/m^3 is the initial concentration. The figures show the saturated zone (carmine red color), the adsorption zone, and the fresh adsorbent zone (navy color) of the column. At the beginning of the process, the entire SB bed is unsaturated, but only 5 min five after, the ACT molecule has been displaced over much of the column. A rapid increase in the ACT concentration is observed within the bed, and it can be seen that approximately 1 cm of bed has been saturated, the mass transfer zone (MTZ) is approximately 13 cm, and there is approximately 9 cm of fresh bed, as seen in the Fig. 6a. At 15 min, the saturated zone grows to 2.5 cm, and the MTZ has reached the end of the column, and the breakthrough time occurs approximately at that time. At 20 and 30 min, the saturated zone is around 4.5 and 14 cm, respectively. It can be seen that this zone grows slowly at first, but between 20 and 30 min, it shows accelerated growth; this happens because in this time interval the slope of the breakthrough curve is formed. Therefore, the saturation of the bed occurred gradually as the mass transfer zone proceeds through the bed at the beginning of the operation. Similar behavior was observed for bed heights of 33 and 43 cm, where the MTZ value was roughly 16.5 and 23 cm, respectively. This shows that MTZ grows as the bed height increases. Also, The MTZ values show that the ACT adsorption rate is slow because the intra and interparticle resistances are considerable [63]. Additionally, due to the CFD model includes the axial dispersion phenomenon, and the simulated breakthrough curves were very similar to the experimental ones, this indicates that this phenomenon is significant, at least at a bed height of 23 cm.

The wall channeling effect was studied with the CFD model. An exponential expression, which expresses the variation bed porosity with radial distance, was added to the CFD model. As can be seen in Fig. 7, the bed porosity increases exponentially as it reaches the wall, this happens since as the SB particles approach the wall of the column, its geometry of packing is interrupted there [54]. This porosity behavior affects the flow distribution of the ACT solution, which causes the velocity near the wall to be higher than in the center region. As a consequence of this phenomenon, the adsorbent SB near the wall reaches saturation much quicker than the center region, as can be seen in Fig. 7. The wall effect is predominant in this adsorption process because the fixed-bed column diameter to SB diameter ratio is low than 30 [53]. In addition, it was observed that the wall channeling effect decreased with the increase of the bed height to SB diameter ratio (H/d_p); at 43 cm of bed height, the difference between the ACT concentration on the wall and the center region was insignificant.

4. Conclusions

Fixed-bed column tests were combined with breakthrough curve modeling to describe the breakthrough curves. The conclusions are as follows:

The analytic models Thomas, Yoon Nelson, Wolborska, Bohart Adams, Wang, and modified dose-response were fitted to the experimental data. The best fit was obtained with the modified dose-response model, and the Wolborska model was the worst model to predict the breakthrough curve. The simulated breakthrough curve by the CFD model was very similar to the experimental breakthrough curve, especially in the initial and transitory region, which could be useful since in practice the adsorbent bed is replaced before a breakthrough of more than 50%. Also, a CFD analysis showed that the fixed-bed column for ACT adsorption in SB has a high mass transfer zone with a slow adsorption rate due to intra and interparticle resistances are considerable, and the mass transfer zone grows as the bed height increases. The CFD simulation showed that the diffusion resistances and axial dispersion phenomenon are relevant in the ACT adsorption into SB, and these must be taken into account in the design of the adsorption columns. In particular, the Knudsen diffusion was more significant compared to the pore diffusion. Finally, the wall channeling effect was relevant with low bed heights but it decreases with higher ones.

CRediT authorship contribution statement

Mayra Vera: Methodology, Conceptualization, Writing - original draft. **Diego Juela:** Data curation, Formal analysis, Validation, Writing - original draft. **Christian Cruzat:** Investigation. **Ma. Eulalia Vanegas:** Funding acquisition, Project administration, Writing - review and editing.

Declaration of Competing Interest

The authors declare that they have no known competing financial interests or personal relationships that could have appeared to influence the work reported in this paper.

Acknowledgements

Authors would like to acknowledge to the Dirección de Investigación de la Universidad de Cuenca (DIUC) for financing through the project DIUC_XIV_2016_037.

References

[1] D.E. Vidal-Dorsch, S.M. Bay, K. Maruya, S.A. Snyder, R.A. Trenholm, B. J. Vanderford, Contaminants of emerging concern in municipal wastewater effluents and marine receiving water, Environ. Toxicol. Chem. 31 (12) (2012) 2674–2682, https://doi.org/10.1002/etc.2004.

[2] C. Song, C. Zhang, L. Fan, L. Qiu, W. Wu, S. Meng, G. Hu, B. Kamira, J. Chen, Occurrence of antibiotics and their impacts to primary productivity in fishponds around tai lake, China, Chemosphere 161 (2016) 127–135, https://doi.org/10.1016/j.chemosphere.2016.07.009.

[3] N. Milić, M. Milanović, N.G. Letić, M.T. Sekulić, J. Radonić, I. Mihajlović, M. V. Miloradov, Occurrence of antibiotics as emerging contaminant substances in aquatic environment, Int. J. Environ. Health Res. 23 (4) (2013) 296–310, https://doi.org/10.1080/09603123.2012.733934.

[4] T. Anumol, A. Vijayanandan, M. Park, L. Philip, S.A. Snyder, Occurrence and fate of emerging trace organic chemicals in wastewater plants in Chennai, India, Environ. Int. 92–93 (2016) 33–42, https://doi.org/10.1016/j.envint.2016.03.022.

[5] D.F. Khamash, A. Voskertchian, P.D. Tamma, I.C. Akinboyo, K.C. Carroll, A. M. Milstone, Increasing clindamycin and trimethoprim-sulfamethoxazole resistance in pediatric staphylococcus aureus infections, J. Pediatr. Infect. Dis. Soc. (2018).

[6] D. Avisar, Y. Lester, H. Mamane, pH induced polychromatic UV treatment for the removal of a mixture of SMX, OTC and CIP from water, J. Hazard. Mater. 175 (1–3) (2010) 1068–1074, https://doi.org/10.1016/j.jhazmat.2009.10.122.

[7] L. Hou, H. Zhang, L. Wang, L. Chen, Y. Xiong, X. Xue, Removal of sulfamethoxazole from aqueous solution by sono-ozonation in the presence of a magnetic catalyst, in: Sep. Purif. Technol, 117, 2013, pp. 46–52, https://doi.org/10.1016/j.seppur.2013.05.014.46–52. DOI: 10.1016/j.seppur.2013.05.014.

[8] D.A. Palacio, B.L. Rivas, B.F. Urbano, Ultrafiltration membranes with three water-soluble polyelectrolyte copolymers to remove ciprofloxacin from aqueous systems, Chem. Eng. J. 351 (2018) 85–93, https://doi.org/10.1016/j.cej.2018.06.099.

[9] M.F.N. Secondes, V. Naddeo, V. Belgiorno, F. Ballesteros, Removal of emerging contaminants by simultaneous application of membrane ultrafiltration, activated carbon adsorption, and ultrasound irradiation, J. Hazard. Mater. 264 (2014) 342–349, https://doi.org/10.1016/j.jhazmat.2013.11.039.

[10] M.C. Tonucci, L.V.A. Gurgel, S.F. de Aquino, Activated carbons from agricultural byproducts (pine tree and coconut shell), coal, and carbon nanotubes as adsorbents for removal of sulfamethoxazole from spiked aqueous solutions: kinetic and thermodynamic studies, Ind. Crops Prod. 74 (2015) 111–121, https://doi.org/10.1016/j.indcrop.2015.05.003.

[11] Y. Tian, B. Gao, V.L. Morales, H. Chen, Y. Wang, H. Li, Removal of sulfamethoxazole and sulfapyridine by carbon nanotubes in fixed-bed columns, Chemosphere 90 (10) (2013) 2597–2605, https://doi.org/10.1016/j.chemosphere.2012.11.010.

[12] X. Yang, R.C. Flowers, H.S. Weinberg, P.C. Singer, Occurrence and removal of pharmaceuticals and personal care products (PPCPs) in an advanced wastewater reclamation plant, Water Res. 45 (16) (2011) 5218–5228.

[13] E. Gracia-Lor, J.V. Sancho, R. Serrano, F. Hernández, Occurrence and removal of pharmaceuticals in wastewater treatment plants at the Spanish Mediterranean area of Valencia, Chemosphere 87 (5) (2012) 453–462, https://doi.org/10.1016/j.chemosphere.2011.12.025.

[14] M.J.M. Bueno, M.J. Gomez, S. Herrera, M.D. Hernando, A. Agüera, A.R. Fernández-Alba, Occurrence and persistence of organic emerging contaminants and priority pollutants in five sewage treatment plants of spain: two years pilot survey monitoring, Environ. Pollut. 164 (2012) 267–273, https://doi.org/10.1016/j.envpol.2012.01.038.

[15] D. Kolpin, E.T. Furlong, M.T. Meyer, E.M. Thurman, S.D. Zaugg, L.B. Barber, H. T. Buton, Pharmaceuticals, hormones, and other organic watereater contaminants in U.S. streams, 1999-2000: a national reconnaissance, Environ. Sci. Technol. 36 (6) (2002) 1202–1211.

[16] M. Petrovic, M. Hernando, M. Díaz -Cruz, D. Barceló, Liquid chromatography-tandem mass spectrometry for the analysis of pharmaceutical residues in environmental samples: a review, J. Chromatogr. A 1067 (2005) 1–14.

[17] A. Yu-Chen Lin, T. Yu-Ting, Occurrence of pharmaceuticals in Taiwan's surface waters: Impact of waste streams from hospitals and pharmaceutical production facilities, Sci. Total Environ. (2009) 3793–3802, https://doi.org/10.1016/j.scitotenv.2009.03.009.

[18] E.W. Godfrey, Pharmaceuticals in on-site sewage effluent and ground water, western Montana, Ground Water 45 (2007) 263–271, https://doi.org/10.1111/j.1745-6584.2006.00288.x.

[19] S. Hokkanen, A. Bhatnagar, M. Sillanpaa, A review on modification methods to cellulose-based adsorbents to improve adsorption capacity, Water Res. 91 (2016) 156–173, https://doi.org/10.1016/j.watres.2016.01.008.

[20] C.P. Silva, G. Jaria, M. Otero, V.I. Esteves, V. Calisto, Waste-based alternative adsorbents for the remediation of pharmaceutical contaminated waters: has a step forward already been taken? Bioresour. Technol. 250 (2018) 888–901, https://doi.org/10.1016/j.biortech.2017.11.102.

[21] N. Feng, X. Guo, S. Liang, Y. Zhu, J. Liu, Biosorption of heavy metals from aqueous solutions by chemically modified orange peel, J. Hazard. Mater. 185 (1) (2011) 49–54, https://doi.org/10.1016/j.jhazmat.2010. 08.114.

[22] A. Witek-Krowiak, R.G. Szafran, S. Modelski, Biosorption of heavy metals from aqueous solutions onto peanut shell as a low-cost biosorbent, Desalination 265 (1–3) (2011) 126–134, https://doi.org/10.1016/j.desal.2010.07.042.

[23] L. Abu-Lail, J.A. Bergendahl, R.W. Thompson, Mathematical modeling of chloroform adsorption onto fixed-bed columns of highly siliceous granular zeolites, Environ. Prog. Sustain. Energy 31 (4) (2012) 591–596, https://doi.org/10.1002/ep.10593.

[24] B. Cheknane, M. Baudu, O. Bouras, F. Zermane, Modeling of basic green 4 dynamic sorption onto granular organo-inorgano pillared clays (GOICs) in column reactor, Chem. Eng. J. 209 (2012) 7–12, https://doi.org/10.1016/j.cej.2012.07.118.

[25] M.J. Meng, Z.P. Wang, L. Ma, M. Zhang, J. Wang, X.H. Dai, Y.S. Yan, Selective adsorption of methylpa- raben by submicrosized molecularly imprinted polymer: batch and dynamic flow mode studies, Ind. Eng. Chem. Res. 51 (45) (2012) 14915–14924, https://doi.org/10.1021/ie301890b.80031-0].

[26] J.T. Nwabanne, P.K. Igbokwe, Kinetic modeling of heavy metals adsorption on fixed bed column, Int. J. Environ. Res. 6 (4) (2012) 945–952. Ohashi, H., Sugawara, T., Kikuchi, K.I., Konno, H., 1981.

[27] H.H. Yi, H. Deng, X.L. Tang, Q.F. Yu, X. Zhou, H.Y. Liu, Adsorption equilibrium and kinetics for SO_2, NO, CO_2 on zeolites FAU and LTA, J. Hazard. Mater. 203–204 (2012) 111–117, https://doi.org/10.1016/j.jhazmat.2011.11.091.

[28] Y. Zhao, Y.M. Shen, L. Bai, S.Q. Ni, Carbon dioxide adsorption on polyacrylamide-impregnated silica gel and breakthrough modeling, Appl. Surf. Sci. 261 (2012) 708–716, https://doi.org/10.1016/j.apsusc.2012.08.085.

[29] F. Augier, C. Laroche, E. Brehon, Application of computational fluid dynamics to fixed bed adsorption calculations: Effect of hydrodynamics at laboratory and industrial scale, Sep. Purif. Technol. 63 (2) (2008) 466–474, https://doi.org/10.1016/j.seppur.2008.06.007.

[30] Y. Tavan, S.H. Hosseini, G. Ahmadi, M. Olazar, Mathematical model and energy analysis of ethane dehydration in two-layer packed-bed adsorption, Particuology 47 (2019) 33–40, https://doi.org/10.1016/j.partic.2018.11.001.

[31] C.R. Wilkin, P. Chang, Correlation of diffusion coefficients in dilute solutions, AIChE J. 1 (2) (1955) 264–270, https://doi.org/10.1002/aic.690010222.

[32] Z. Xu, J.G. Cai, B.C. Pan, Mathematically modeling fixed-bed adsorption in aqueous systems, J. Zhejiang Univ. Sci. A 14 (3) (2013) 155–176, https://doi.org/10.1631/jzus.A1300029.

[33] H. Thomas, Heterogeneous ion exchange in a flowing system, J. Am. Chem. Soc. 66 (1944) 1664–1666.

[34] H.C. Thomas, Chromatography: a problem in kinetics, Ann. N. Y. Acad. Sci. 49 (1948) 161–182, https://doi.org/10.1111/j.1749-6632.1948.tb35248.x.

[35] G. Yan, T. Viraraghavan, M. Chen, A new model for heavy metal removal in a biosorption column, Adsorpt. Sci. Technol. 19 (2001) 25–43, https://doi.org/10.1260/0263617011493953.

[36] A.D. Dorado, X. Gamisans, C. Valderrama, M. Sole, C. Lao, Cr(III) removal from aqueous solutions: a straightforward model approaching of the adsorption in a fixed-bed column, J. Environ. Sci. Health A Toxic. /Hazard. Subst. Environ. Eng. 49 (2014) 179–186, https://doi.org/10.1080/10934529.2013.838855.

[37] Y.H. Yoon, Application of gas adsorption kinetics I. A theoretical model for respirator cartridge service life. Am. Ind. Hyg. Assoc. J. 45 (1984) 509–516.

[38] S. Ayoob, A.K. Gupta, Sorptive response profile of an adsorbent in the defluoridation of drinking water, Chem. Eng. J. (2007), https://doi.org/10.1016/j.cej.2007.02.013.

[39] G.S. Bohart, E.Q. Adams, Some aspects of the behavior of charcoal with respect to chlorine, J. Am. Chem. Soc. 42 (1920) 523–544, https://doi.org/10.1021/ja01448a018.

[40] J. Goel, K. Kadirvelu, C. Rajagopal, V. Kumar Garg, Removal of lead(II) by adsorption using treated granular activated carbon: batch and column studies, J. Hazard. Mater. 125 (2005) 211–220, https://doi.org/10.1016/j.jhazmat.2005.05.032.

[41] M. Calero, F. Hernz, G. Blazquez, G. Tenorio, M.A. Martín-Lara, Study of Cr (III) biosorption in a fixed-bed column, J. Hazard. Mater. 171 (2009) 886–893, https://doi.org/10.1016/j.jhazmat.2009.06.082.

[42] Y. Sag, Y. Aktay, Application of equilibrium and mass transfer models to dynamic removal of Cr(VI) ions by Chitin in packed column reactor, Process Biochem. 36 (2001) 1187–1197, https://doi.org/10.1016/S0032-9592(01)00150-9.

[43] Y.H. Wang, S.H. Lin, R.S. Juang, Removal of heavy metal ions from aqueous solutions using various low-cost adsorbents, J. Hazard. Mater. 102 (2–3) (2003) 291–302, https://doi.org/10.1016/S0304-3894(03)00218-8.

[44] A. Wolborska, Adsorption on activated carbon of p-nitrophenol from aqueous solution, Water Res. 23 (1) (1989) 85–91, https://doi.org/10.1016/0043-1354(89)90066-3.

[45] A. Wolborska, Determination of mass transfer coefficient adsorption in a fixed bed, Inz. Chem. I Proces. 4 (1989) 545–556.

[46] A. Wolborska, P. Pustelnik, A simplified method for determination of the break-through time of an adsorbent layer, Water Res. 30 (11) (1996) 2643–2650, https://doi.org/10.1016/S0043-1354(96)00166-2.

[47] A.S. Mestre, E. Tyszko, M.A. Andrade, M. Galhetas, C. Freire, A.P. Carvalho, Sustainable activated carbons prepared from a sucrose-derived hydrochar: remarkable adsorbents for pharmaceutical compounds, RSC Adv. 5 (25) (2015) 19696–19707, https://doi.org/10.1039/C4RA14495C.
[48] F. Augier, C. Laroche, E. Brehon, Application of computational fluid dynamics to fixed bed adsorption calculations: Effect of hydrodynamics at laboratory and industrial scale, Sep. Purif. Technol. 63 (2) (2008) 466–474, https://doi.org/10.1016/j.seppur.2008.06.007.
[49] H. Ohashi, T. Sugaware, K. Kikuchi, H. Konno, Correlation of liquid-side mass transfer coefficient for single particles and fixed beds, J. Chem. Eng. 14 (6) (1981) 433–438, https://doi.org/10.1252/jcej.14.433.
[50] Y. Tavan, S.H. Hosseini, G. Ahmadi, M. Olazar, Mathematical model and energy analysis of ethane dehydration in two-layer packed-bed adsorption, Particuology 47 (2019) 33–40, https://doi.org/10.1016/j.partic.2018.11.001.
[51] C.R. Wilke, P. Chang, Correlation of diffusion coefficients in dilute solutions, AIChE J. 1 (2) (1955) 264–270, https://doi.org/10.1002/aic.690010222.
[52] S.M. White, C.L. Tien, Analysis of flow channeling near the wall in packed beds, Wärme- und Stoffübertrag. 21 (1987) 291–296, https://doi.org/10.1007/BF01009290.
[53] Y. Xiao, S. Qiu, Q. Zhao, Y. Zhu, C.B. Godiya, G. He, Numerical simulation of low-concentration CO_2 adsorption on fixed bed using finite element analysis, Chin. J. Chem. Eng. (2020), https://doi.org/10.1016/j.cjche.2020.08.012.
[54] F. Mousazadeh, H.E.A. van Den Akker, R.F. Mudde, Direct numerical simulation of an exothermic gas-phase reaction in a packed bed with random particle distribution, Chem. Eng. Sci. 100 (2013) 259–265, https://doi.org/10.1016/j.ces.2013.02.019.
[55] D.C. Sau, K.C. Biswal, Computational fluid dynamics and experimental study of the hydrodynamics of a gas–solid tapered fluidized bed, Appl. Math. Model. 35 (2011) 2265–2278, https://doi.org/10.1016/j.apm.2010.11.037.
[56] O. Lorphensri, D.A. Sabatini, T.C. Kibbey, K. Osathaphan, C. Saiwan, Sorption and transport of acetaminophen, 17alpha-ethynyl estradiol, nalidixic acid with low organic content aquifer sand, Water Res. 41 (10) (2007) 2180–2188.
[57] B.M. Dalfior, Evaluation of coconut mesocarp for removing paracetamol in aqueous medium by batch experiments, Analytica 63 (2013) 53–58.
[58] A. Flores, M. Belisário, R. Galazzi, D. Balthazar, M. Pereira, J. Ribeiro, Evaluation of two bioadsorbents for removing paracetamol from aqueous media, Electron. J. Biotechnol. 14 (6) (2011).
[59] K.H. Chu, Breakthrough curve analysis by simplistic models of fixed bed adsorption: in defense of the century-old Bohart-Adams model, Chem. Eng. J. 380 (2020), 122513, https://doi.org/10.1016/j.cej.2019.122513.
[60] K.H. Chu, Fitting the Gompertz equation to asymmetric breakthrough curves, J. Environ. Chem. Eng. 8 (2020), 103713, https://doi.org/10.1016/j.jece.2020.103713.
[61] M. Izquierdo, C. Gabaldón, P. Marzal, F.J. Álvarez-Hornos, Modeling of copper fixed-bed biosorption from wastewater by *Posidonia oceanica*, Bioresour. Technol. 101 (2010) 510–517, https://doi.org/10.1016/j.biortech.2009.08.018.
[62] J.M.P.Q. Delgado, A critical review of dispersion in packed beds, Heat Mass Transf. 42 (2006) 279–310, https://doi.org/10.1007/s00231-005-0019-0.
[63] H. Patel, Fixed-bed column adsorption study: a comprehensive review, Appl. Water Sci. 9 (3) (2019), 45, https://doi.org/10.1007/s13201-019-0927-7.
[64] Diego M. Juela, Comparison of the adsorption capacity of acetaminophen on sugarcane bagasse and corn cob by dynamic simulation, Sustain. Environ. Res. 30 (1) (2020), https://doi.org/10.1186/s42834-020-00063-7. In press.